Applied Thermal Engineering 206 (2022) 118045

Contents lists available at ScienceDirect

Applied Thermal Engineering

journal homepage: www.elsevier.com/locate/ate

Research paper

# Experimental validation and development of an advanced computational model of a transcritical carbon dioxide vapour compression cycle with a thermoelectric subcooling system

Álvaro Casi [a], Patricia Aranguren [a], Daniel Sanchez [b], Miguel Araiz [a,*], Ramón Cabello [b], David Astrain [a]

[a] Department of Engineering, Institute of Smart Cities, Public University of Navarre, Campus de Arrosadia s/n E-31006, Pamplona, Spain
[b] Department of Mechanical Engineering and Construction, Jaume I University, Campus de Riu Sec s/n E-12071 Castellón, Spain

ARTICLE INFO

*Keywords:*
Carbon dioxide
Thermoelectric subcooling
Computational model
Experimental validation

ABSTRACT

The inclusion of a thermoelectric subcooler as an alternative to increment the performance of a vapour compression cycle has been proved promising when properly designed and operated for low-medium power units. In this work, a computational model that simulates the behaviour of a carbon dioxide transcritical vapour compression cycle in conjunction with a thermoelectric subcooler system is presented. The computational tool is coded in Matlab and uses Refprop V9.1 to calculate the properties of the refrigerant at each point of the refrigeration cycle. Working conditions, effect of the heat exchangers of the subcooling system, temperature dependent thermoelectric properties, thermal contact resistances and the four thermoelectric effects are taken into account to increment its accuracy. The model has been validated using experimental data to prove the reliability and accuracy of the results obtained and shows deviations between the ±7% for the most relevant outputs. Using the validated computational tool a 13.6 % COP improvement is predicted when optimizing the total number of thermoelectric modules of the subcooling system. The computational experimentally validated tool is properly fit to aid in the design and operation of thermoelectric subcooling systems, being able to predict the optimal configuration and operation settings for the whole refrigeration plant.

## 1. Introduction

Carbon dioxide ($CO_2$) refrigeration systems were proposed as a natural alternative to the use of artificial refrigerants by Professor Lorentzen in 1995 [1] and recently, $CO_2$ had risen in popularity as a refrigerant due to its zero Ozone Depletion Potential, negligible Global Warming Power, non-toxicity, non-flammability, availability and superior thermal properties [2]. Despite its many advantages, $CO_2$ vapour compression systems normally operate under transcritical conditions, decreasing the coefficient of performance (COP) of the system as a result of exergy losses [3,4]. To compensate this decrease on the COP, new systems have been developed such as: internal heat exchangers [5], parallel compressors [6], multi-stage compression arrangements [7,8], ejectors [9–11], expanders [12], thermoelectric subcoolers [13], mechanical subcoolers [14,15] or a combination of these systems, for example, a thermoelectric subcooler with expander or a thermoelectric subcooler with ejector [16,17].

Thermoelectric subcooling systems, due to their robustness, compactness, modularity and simplicity, had been the focus of recent studies and affirm themselves as a viable possibility for low-medium power units, where most of the other alternatives present complex control systems or high economical costs. A thermoelectric subcooler (TESC) is based on the use of thermoelectric modules (TEMs) that take advantage of the Peltier effect to transform electrical power into a heat flux without the need of a working fluid, cooling the carbon dioxide at the outlet of the gas-cooler in order to increase the specific cooling capacity and COP of the thermodynamic cycle.

The inclusion of a TESC in a $CO_2$ transcritical cycle has been theoretically analysed and simulated by different authors over the past few years. Sarkar predicted an increase in the COP of 25.6% and a reduction of the discharge pressure of 15.4% using a computational model [18]. Yazawa et al. predicted an improvement of 12–13% on maximum cooling performance in a data centre cooling application [19]. Jamali et al. presented a mathematical model that predicts improvements of up to 19% on the COP of the refrigeration cycle [20]. Kwan et al. studied the effect of including 1 or 2 thermoelectric subcooling devices in a transcritical carbon dioxide cycle and predicted improvements in

* Correspondence to: Engineering Department. Public University of Navarre, Campus de Arrosadia s/n, 31006 Pamplona, Spain.
*E-mail address:* miguel.araiz@unavarra.es (M. Araiz).

https://doi.org/10.1016/j.applthermaleng.2022.118045
Received 5 August 2021; Received in revised form 23 December 2021; Accepted 4 January 2022
Available online 23 January 2022
1359-4311/© 2022 The Author(s). Published by Elsevier Ltd. This is an open access article under the CC BY-NC-ND license (http://creativecommons.org/licenses/by-nc-nd/4.0/).

**Nomenclature**

**Variables**

| | |
|---|---|
| $A$ | Area ($m^2$) |
| $c$ | Specific heat (kJ/kgK) |
| $COP$ | Coefficient of performance |
| $e$ | Thickness (m) |
| $f$ | Darcy friction factor |
| $h$ | Enthalpy (kJ/kg) |
| $hc$ | Heat transfer coefficient ($W/m^2K$) |
| $k$ | Thermal conductivity (W/mK) |
| $\dot{m}$ | Mass flow rate (kg/h) |
| $N$ | Number of subcooling block |
| $Nu$ | Nusselt number |
| $NUSH$ | Non useful superheating ($K$) |
| $P$ | Pressure (bar) |
| $Pr$ | Prandtl number |
| $\dot{Q}$ | Heat transfer rate (W) |
| $R$ | Thermal Resistance (K/W) |
| $Re$ | Reynolds number |
| $RH$ | Relative humidity (%) |
| $Sub$ | Subcooling (K) |
| $T$ | Temperature (°C) |
| $T'$ | Calculated temperature (°C) |
| $USH$ | Useful superheating (K) |
| $V$ | Voltage (V) |
| $\dot{V}$ | Volumetric flow rate ($m^3/s$) |
| $v$ | Specific volume ($m^3/kg$) |
| $\dot{W}$ | Power consumption (W) |
| $Z$ | Thermal impedance ($m^2K/W$) |

**Subscripts and superscripts**

| | |
|---|---|
| 0 | At the evaporator |
| $amb$ | Ambient |
| $block$ | Subcooling block |
| $CO2$ | Carbon dioxide |
| $cold$ | Cold side of the TEM |
| $comp$ | Compressor |
| $cont$ | Contact |
| $evap$ | Evaporator |
| $exper$ | Experimental |
| $fan$ | Fans of the finned heat exchangers |
| $g$ | Global |
| $gc$ | Gas cooler |
| $gly$ | Glycol and water mixture |
| $hot$ | Hot side of the TEM |
| $hx$ | Heat exchanger |
| $in$ | Inlet |
| $ins$ | Insulation |
| $N$ | Number of subcooling block |
| $out$ | Outlet |
| $p$ | At constant pressure |
| $simul$ | Simulated |
| $TEM$ | Thermoelectric module |
| $TESC$ | Thermoelectric subcooler |
| $tim$ | Thermal interface material |
| $v$ | Volumetric |

**Greek symbols**

| | |
|---|---|
| $\eta$ | Efficiency |
| $\varepsilon$ | Heat exchanger efficiency |

the COP of 6.24% when using 2 subcooling thermoelectric devices compared to 1 [21].

Although these theoretical studies and computation models contribute with relevant information and increase the knowledge of this technology, the studies do not perform an experimental validation of the computational methodology to probe the reliability of the results. The only model present in the literature that compares its results is the one developed by Jamali et al. [20], however, the comparative is made with data obtained with other computational models and this does no probe the reliability of the model. In all cases, the computational data obtained through the theoretical works presented in the literature have not been compared with real experimental data to prove the consistency of the computational methodologies. Therefore the information obtained as a result of these studies is not totally reliable. In addition, the published theoretical studies do not take into account key factors that have been proven relevant when thermoelectric systems are simulated such as: the effect of the heat exchangers of the subcooling system [22], temperature dependence of the thermoelectric properties [23], the auxiliary consumption of the heat exchangers [24] or the voltage that needs to be supplied to the TEMs to work at optimum conditions [13].

Furthermore, the effects of including a TESC depend on many variables related to the vapour compression cycle and the thermoelectric subcooling system such as: discharge pressure, volumetric capacity of the compressor, efficiency of the gas cooler, number of TEMs, voltage supplied to the TEMs or thermal resistance value of the heat exchangers. Hence, the final result of including a TESC depends on the characteristics and operation settings of both the vapour compression cycle and the thermoelectric subcooling system. Therefore, in order to predict optimum working conditions of the combined system, both systems need to be taken into account together and thus, have to be simulated in conjunction. This effect that the working conditions have on the performance of the combined cycle and the interdependence between the vapour compression cycle and the subcooling system have not yet been studied in the literature. In fact, when the operation settings are poorly managed, the inclusion of a thermoelectric subcooling system can even be counterproductive for the COP of the whole system, which remarks the necessity of properly predicting the optimum working conditions.

This work presents an advanced computational model that simulates the operation of a transcritical $CO_2$ refrigeration cycle in conjunction with a thermoelectric subcooling system. For the first time, several effects and key aspects for the simulation of thermoelectric systems have been taken into account in the combined model. In addition, the computational model has been validated using real experimental data to prove the reliability of the results obtained and thus, sets an unmatched precedent for future models that simulate this combination of technologies. The advanced model takes into account all the thermoelectric effects that take place in a thermoelectric module (TEM), the effect of the heat exchangers of the thermoelectric subcooling system, contact thermal resistances, auxiliary consumption of the heat exchangers or temperature dependent thermoelectric properties amongst others. The model has been validated using previous experimental data, proving its reliability and the accuracy of the results. The developed validated computational tool is remarkable, been able to aid in the design of transcritical $CO_2$ refrigeration cycles that include a thermoelectric subcooling system, been able to predict optimum working

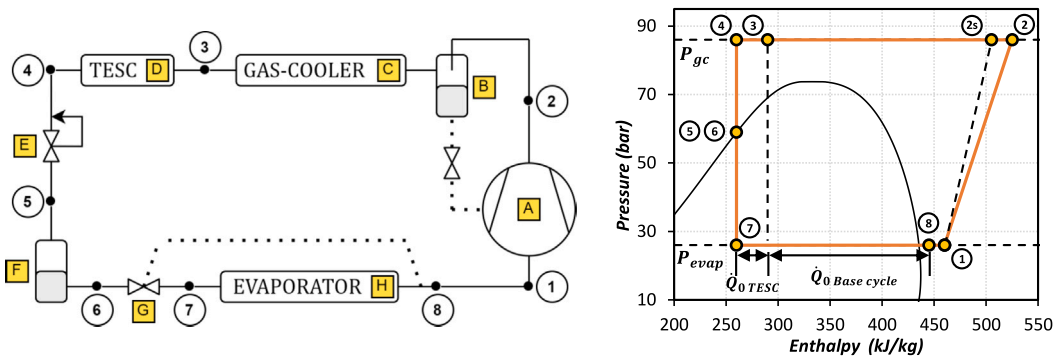


**Fig. 1.** Refrigeration test bench with thermoelectric subcooling system schematic (left) and P–h diagram (right)

conditions for the combined system. Lastly, using the computational model, the optimum number of TEMs for the experimental setup is predicted.

## 2. Experimental system

The objective of the computational model developed in this work is to properly simulate the operation of a carbon dioxide transcritical refrigeration cycle that includes a novel thermoelectric subcooling system to improve its efficiency. In this section, the experimental test bench used to validate the computational model is described.

### 2.1. Refrigeration test bench

The refrigeration test bench consists of a single-stage vapour compression system that incorporates a thermoelectric subcooling system. Fig. 1 shows an schematic of the test bench and a P–h diagram of the thermodynamic cycle.

The system is designed to use carbon dioxide as a refrigerant under transcritical conditions, making use of a two-stage expansion process the system is able to control the pressure of the gas-cooler and the useful superheating of the evaporator. The test bench main elements (highlighted in Fig. 1 with letters from A to H) are: an hermetic compressor (A), SANDEN SRFCA, with a cubic capacity of $1.1\,cm^3$ and a nominal rotation speed of 2900 rpm at 50 Hz; a coalescent filter (B), SWAGELOK SS-6TF-F6-05, that separates the lubricating oil from the compressor; a finned gas-cooler (C), SEREVA CA-32, that consists of 8 copper pipes disposed in 4 steps, a transfer area with fins of $2.15\,m^2$ and, provided with an axial fan which circulates ambient air through its coil; a thermoelectric subcooling system (D) which consists of 8 thermoelectric modules separated in 4 subcoooling blocks and is further explained in detail in Section 2.2; an electronic back-pressure valve (E), CAREL E2V03, to control the pressure of the gas-cooler;custom built accumulation tank (F) of 3.7 L to ensure that the inlet of the second electronic expansion valve is saturated liquid; an electronic thermostatic valve (G), CAREL E2V03, that controls the useful superheating at the outlet of the evaporator; and lastly, a brazed-plate evaporator (H), Alfa Laval AXP14-50H-F, with a surface area of $0.576\,m^2$ in which the refrigerant evaporates using a mixture of water and ethylene glycol (49% in mass) as the secondary fluid.

The mixture of water and glycol that flows through the evaporator is heated by a 1500 W resistor regulated by a closed loop PID controller in order to maintain the conditions of the evaporator constant. The volumetric flow is controlled using a pump alongside a metering valve. Finally, in order to diminish the effects of heat exchange with the exterior, the test bench has been thoroughly insulated using foam with a thermal conductivity of 0.0036 W/mK according to ISO 13787, this can be observed in detail in Fig. 2.

### 2.2. Thermoelectric subcooler (TESC)

The main purpose of the TESC is to improve the COP of the refrigeration system by efficiently cooling the refrigerant at the outlet of the gas-cooler, increasing the specific cooling power at the evaporator and therefore, the total cooling power of the refrigeration system. For that, 4 blocks of subcooling are connect in series at the outlet of the gas-cooler with 2 TEMs per block (8 TEMs in total).

The elements that compose each subcooling block can be observed in detail in Fig. 3 and are the following: a handcrafted solid copper block heat exchanger (1) of $60 \times 74 \times 10\,mm^3$ with an interior drilled path that provides an internal heat exchange area of $0.0037\,m^2$, the hydraulic diameter drilled path is 3 mm; 2 bismuth-telluride TEMs RC-8-01L (2) from Marlow Industries, the semi-conductors present a cross section area of $1.4 \times 1.4\,mm^2$ and a length of 1.3 mm, the ZT provided by the manufacturer is 0.73 at a cold side temperature of 27 °C, the total surface area of the modules is $40 \times 40\,mm^2$ and each one consists of 127 thermocouples; 2 aluminium finned heat exchangers (3), Arctic Alpine 64 GT, with 35 fins and a surface area of $0.16\,m^2$; and finally, 2 axial fans (4) of 80 mm of diameter with a power consumption of 1.4 W each.

The block is assembled placing the cold side of the TEMs on both sides of the copper block and then positioning the finned heat exchangers on the hot side of both TEMs. Thermal grease with a thermal conductivity of 5 W/mK is applied in both sides of the TEMs in order to minimize thermal contact resistances between the TEMs, the copper block and the finned dissipators. The system is clamped with 4 screws through the finned dissipators applying a torque of 1 Nm as specified by the manufacturer and welded to the refrigeration facility through oxyacetylene welding. All the free surfaces exposed to the surroundings are covered with foam in order to minimize heat transfer. Finally, the TEMs are connected electrically in parallel to an adjustable power supply.

The refrigerant at the outlet of the gas-cooler flows through the internal path of the copper block heat exchanger (1) and gets subcooled due to the Peltier effect produced on the TEMs (2). The modules, when supplied with voltage, force a heat flux that extracts energy from the refrigerant cooling down the $CO_2$. The heat is dissipated into the ambient through the aluminium finned heat exchangers (3) helped by the forced convection produced by the fans (4). The subcooling produces an increase in specific cooling capacity and introduces the consumption of the TEMs on the refrigeration system. When optimized and properly managed, the increases in specific cooling capacity compensates the increase in power consumption and the COP of the cycle is enhanced as a consequence.

### 2.3. Data acquisition and measurement probes

The refrigerant plant is fully monitored using a data acquisition system alongside several measurement probes and sensors. The probes

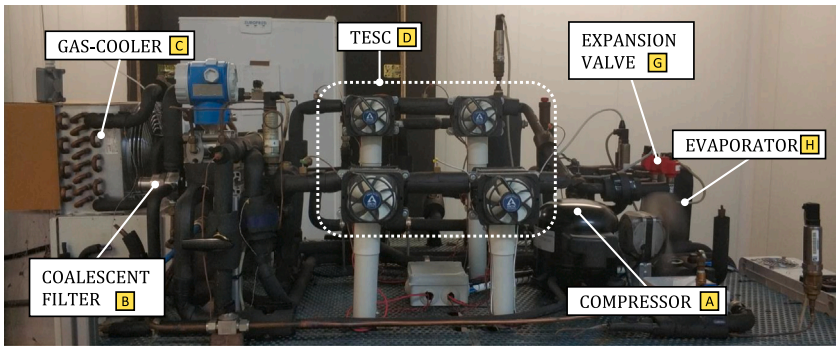


**Fig. 2.** Experimental refrigeration test bench.

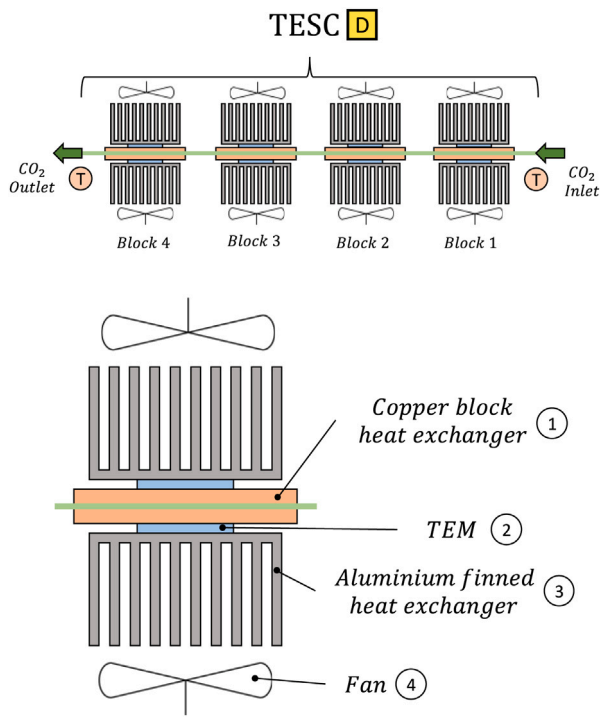


**Fig. 3.** Schematic of the thermoelectric subcooling system.

**Table 1**
Main characteristics of the measurement equipment.

| Probe | Measured variable | Accuracy |
|---|---|---|
| Thermocouple T | Temperature (°C) | ±0.5 °C |
| Pressure gauge | Pressure (bar) | ±0.6% of full scale |
| Coriolis flowmeter | Mass flow rate (kg/h) | ±0.5% of reading |
| Network analyser | Power consumption (W) | ±0.5% of reading |
| Hygrometer | Relative humidity (%) | ±2% RH |
| Digital multimeter | DC voltage (V) | ±0.5% of reading |
| Digital multimeter | DC current (A) | ±0.2% of reading |

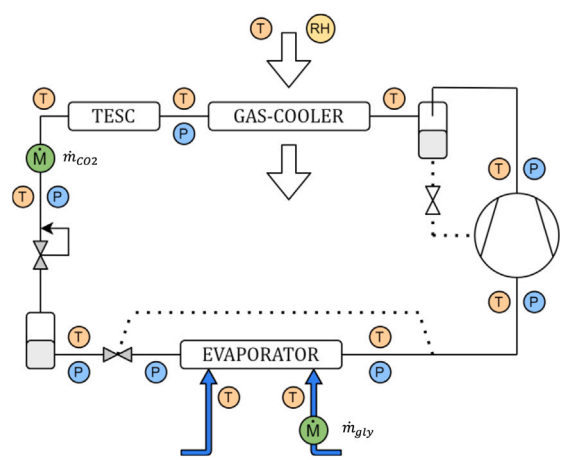


**Fig. 4.** Schematic diagram of the refrigeration plant and locations of probes and sensors.

location can be seen in detail in Figs. 3 and 4. Temperature is measured using T-type thermocouples ($T$); pressure is measured with pressure gauges ($P$); mass flow is measured using a Coriolis mass flowmeter ($\dot{M}$) for both, the refrigerant ($CO_2$) and the secondary fluid (water–glycol mixture); electrical power consumption from the compressor is measured using a network analyser; relative humidity is measured using an hygrometer ($RH$); and lastly, voltage and current at the TEMs and the fans are measured using digital multimeters. The main characteristics of the measurement equipment are collected in Table 1.

Measurements are recorded for the last 20 min of the test after stationary state conditions are reached, registering data in 10 s intervals. The information is recorded in a personal computer, processed using Excel, Matlab, Refprop v9.1 and SecCool v.1.33.

### 2.4. Experimental methodology

The tests have been performed according to ISO 23953 class IV conditions ($T_{amb}$ = 30 °C and $RH_{amb}$ = 55%). In addition, more working parameters were adjusted in order to properly set controlled working conditions in the refrigeration test bench: the evaporation level ($T_{evap}$) was maintained at −10 °C, the useful superheating degree ($USH$) was set to 4 K and the water–glycol mass flow rate ($\dot{m}_{gly}$) was controlled at a value of 100 kg/h. The experimental test bench was tested inside a climatic chamber to maintain uniform climatic class IV conditions, therefore, the heat rejection conditions for the thermoelectric subcooling system were the same as for the gas-cooler.

The refrigeration test bench is tested first without the TESC. For that, the discharge pressure is fixed to 82.1, 85.0, 86.6, 89.9 and 93.8 bar, the optimal working pressure obtained for the base cycle of the refrigeration test bench was 86.6 bar [25]. Under this working conditions the cooling capacity of the system is 289.0 W with a power consumption of the compressor of 279.5 W and a COP of 1.03. To assess the basic operation of the system with the TESC, experiments were performed with the TESC at 2 different levels of discharge pressure: 83 and 86.6 bar. Moreover, the voltage supplied to the TEMs and the voltage supplied to the fans of the heat exchangers of the TESC were varied during the tests to evaluate the effect of the subcooling system under different working conditions. Voltage supplied to the TEMs was set to 0.5, 1, 1.5, 2, 2.5, 3, 3.5, 4, 6 and 8 V, while voltage to the fans was fixed to 6, 9 and 12 V. Table 2 summarizes the working conditions

**Table 2**
Working conditions of the experimental tests of the transcritical $CO_2$ refrigeration plant.

| | $T_{amb}$ (°C) | $HR_{amb}$ (%) | $T_{evap}$ (°C) | $USH$ (K) | $\dot{m}_{gly}$ (kg/h) | $P_{gc}$ (bar) | $V_{TEMs}$ (V) | $V_{fan}$ (V) |
|---|---|---|---|---|---|---|---|---|
| Without TESC | 30 | 55 | −10 | 4 | 100 | 82.1, 85.0, 86.6, 89.9 & 93.8 | – | – |
| With TESC | 30 | 55 | −10 | 4 | 100 | 83 & 86.6 | 0.5, 1, 1.5, 2, 2.5, 3, 3.5, 4 & 6 | 6, 9 & 12 |

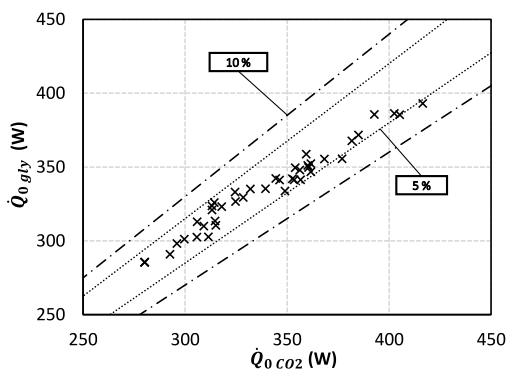


**Fig. 5.** Experimental data validation with measured data at the evaporator between the refrigerant (CO2) and the secondary fluid (water–glycol mixture).

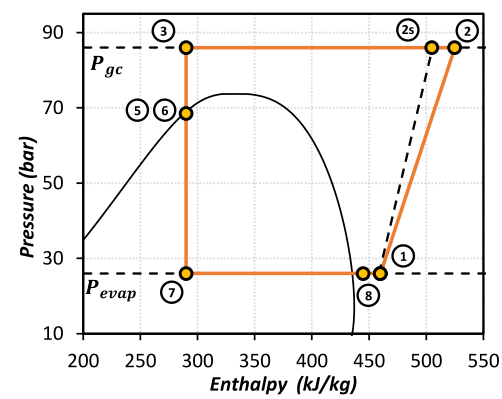


**Fig. 6.** P–h diagram of the transcritical base cycle.

for the experimental tests. These experimental data has already been published and discussed in previous work [13], and is used to validate the computational model developed.

In order to prove the reliability of all the experimental tests, the cooling capacity of the whole refrigeration system ($\dot{Q}_0$) was calculated in 2 ways: using data from the refrigerant as in Eq. (1) and utilizing data from the secondary fluid as in Eq. (2).

$$\dot{Q}_{0\ CO2} = \dot{m}_{CO2} \cdot (h^{out}_{evap} - h^{in}_{evap}) \tag{1}$$

$$\dot{Q}_{0\ gly} = \dot{m}_{gly} \cdot c_{p\ gly} \cdot (T^{in}_{gly} - T^{out}_{gly}) \tag{2}$$

In Eq. (1) the mass flow rate of the refrigerant ($\dot{m}_{CO2}$) is measured by a Coriolis mass flow meter and the enthalpies at the inlet and outlet of the evaporator ($h^{in}_{evap}$ and $h^{out}_{evap}$) are calculated using Refprop v9.1 along the temperatures and pressures of each point. In Eq. (2) the mass flow rate of the water–glycol mixture ($\dot{m}_{gly}$) is obtained using a Coriolis mass flow meter, water–glycol temperatures ($T^{in}_{gly}$ and $T^{out}_{gly}$) are obtained by immersion temperature probes, and lastly, the specific heat of the mixture is calculated using the average temperature of the secondary fluid at the evaporator along with the software SecCool v.1.33. The results obtained using these 2 equations are compared in Fig. 5 for all the tests performed. The discrepancy between both results is mostly between the ±5% with a maximum difference of 5.6% of cooling capacity. These differences are of the same order as the experimental errors cause by the measuring equipment. This clearly shows a good agreement between the data collected with the refrigerant and the data collected with the secondary fluid which proves the reliability of the results obtained during the experimental tests. The experimental data obtained during the tests, which has been proven reliable, is used to validate the computational model and is shown alongside the simulated data in Section 4.

## 3. Computational model

The model aims to simulate the behaviour of a carbon dioxide vapour compression cycle working under transcritical conditions combined with a thermoelectric subcooling system, resolving the thermodynamic cycle and calculating the global coefficient of performance of the combined system.

The inclusion of a subcooling device in a vapour compression system modifies the optimum working pressure for the refrigeration plant and predicting this optimum pressure becomes a necessity to optimize the whole cooling system. In addition, in a thermoelectric subcooling system, the efficiency and the total subcooling produced are directly affected by the discharge pressure level of the cycle, the number of TEMs or the voltage supplied to these TEMs. Summarizing, the optimum working conditions for the whole refrigeration system are interconnected between the vapour compression system and the thermoelectric subcooling system and in order to properly predict the optimum working conditions of the combined system a complete computational model that takes into account both systems needs to be developed.

The complete model presented in this work consists of 2 main submodels that work together: the base cycle model explained in Section 3.1 and the thermoelectric refrigeration model described in Section 3.2. Then, in Section 3.3 a detailed explanation in how the two submodels interact with each other is presented.

### 3.1. Base cycle model

The base cycle model simulates a simple vapour compression cycle that uses carbon dioxide under transcritical conditions as the one shown in Fig. 6. It is coded in Matlab and calculates the pressure, temperature and enthalpy of each point, mass flow through the installation, power consumption of the compressor, cooling power produced at the evaporator and COP of the refrigeration system. To solve the thermodynamic cycle the following inputs are needed: evaporation level ($T_{evap}$), useful superheating ($USH$), non-useful superheating ($NUSH$), gas-cooler pressure ($P_{gc}$) and ambient temperature ($T_{amb}$). Refprop v9.1 is used to obtain the properties and thermodynamic state of points of interest.

The model starts calculating the pressure of the vapour saturated state at the evaporator using the temperature of the evaporation level. The pressure calculated corresponds to $P_{evap}$ which is the same for points 1, 7 and 8. Temperature of point 8 is obtained adding the useful superheating (4 K) to the evaporation temperature as in Eq. (3). With the already calculated pressure of the evaporator the enthalpy of point 8 (outlet of the evaporator) is calculated. The temperature of point 1 is obtained adding the non-useful superheating, which has been set to 12 K, to the temperature of point 8 through Eq. (4).

$$T_8 = T_{evap} + USH \tag{3}$$

$$T_1 = T_8 + NUSH \tag{4}$$

**Table 3**
Experimental coefficients for the compressor: $P_{evap}$ $(bar) = [25–35]$, $P_{gc}$ $(bar) = [60 - 100]$ and $T_1$ (°C) = [−2.5–35.5] [26].

| Volumetric efficiency ($\eta_v$) | Global efficiency ($\eta_g$) |
|---|---|
| $a_0 = -0.0547370788479$ | $b_0 = -0.1889443598024$ |
| $a_1 = 0.0376339677943$ | $b_1 = 0.0220821533615$ |
| $a_2 = -0.0042826165592$ | $b_2 = -0.0000985743589$ |
| $a_3 = 0.0025546148674$ | $b_3 = 0.0021264774317$ |
| Max. deviation ($\eta_v$) = 6.5% | Max. deviation ($\eta_g$) = 7.3% |

**Table 4**
Experimental coefficients for the efficiency of the gas-cooler $T_{amb} = 30$ °C, $RH_{amb} = 55\%$ and $P_{gc}$ $(bar) = [73.8–95]$ [25].

| Efficiency of the gas-cooler ($\varepsilon_{gc}$) | |
|---|---|
| $c_0 = -13.0995846550$ | $c_1 = 0.4454496093$ |
| $c_2 = 0.0047139137$ | $c_3 = 0.0000166648$ |
| Max. deviation ($\varepsilon_{gc}$) = 0.8% | |

The compressor is defined using adjusted expressions from already published data [26]. The expressions can be seen in Eq. (5) and Eq. (6), the coefficients and the maximum deviations obtained are listed in Table 3. The enthalpy of point 2s is obtained with the entropy of point 1 and the discharge pressure (gas-cooler pressure), which is the same for points 2, 2s and 3. Using the volumetric efficiency of the compressor the mass flow rate is calculated as shown in Eq. (7), then the consumption of the compressor is obtained using Eq. (8).

$$\eta_v = a_0 + a_1 \cdot P_{evap} + a_2 \cdot P_{gc} + a_3 \cdot T_1 \tag{5}$$

$$\eta_g = b_0 + b_1 \cdot P_{evap} + b_2 \cdot P_{gc} + b_3 \cdot T_1 \tag{6}$$

$$\dot{m}_{CO2} = \frac{\dot{V}_{comp}}{v_1 \cdot \eta_v} \tag{7}$$

$$\dot{W}_{comp} = \frac{\dot{m}_{CO2} \cdot (h_{2s} - h_1)}{\eta_g} \tag{8}$$

Point 3 is calculated using Eq. (10) where the efficiency of the gas-cooler is obtained through previous experimental data [25] and is introduced as a function of the gas cooler pressure as in Eq. (9), the coefficients and the maximum deviations are listed in Table 4. The enthalpy for points 5, 6 and 7 is the same as that of point 3 and therefore, the cycle resolved.

$$\varepsilon_{gc} = c_0 - c_1 \cdot P_{gc} + c_2 \cdot {P_{gc}}^2 + c_3 \cdot {P_{gc}}^3 \tag{9}$$

$$T_3 = T_2 - \varepsilon_{gc} \cdot (T_2 - T_{amb}) \tag{10}$$

Using the mass flow rate and the enthalpies of points 7 and 8 the cooling power of the refrigeration cycle is calculated as shown in Eq. (11). Finally, using Eq. (12) the COP of the cycle is obtained.

$$\dot{Q}_0 = \dot{m}_{CO2} \cdot (h_8 - h_7) \tag{11}$$

$$COP = \frac{\dot{Q}_0}{\dot{W}_{Comp}} \tag{12}$$

To test the reliability of the base cycle model on its own, the results obtained using the model are compared with experimental data of the refrigeration test bench working without the TESC. The comparative between the base cycle model and the experimental data is summarized in Table 5, where the experimental and simulated data are listed with the deviation obtained between both values. The variables compared in the table are: temperature at the outlet of the evaporator, temperature at the inlet of the compressor, temperature at the outlet of the compressor, temperature at the outlet of the gas-cooler, evaporation pressure, efficiency of the gas-cooler, mass flow rate of the refrigerant, cooling power, power consumption and COP. The differences between the experimental data and the simulated data is expressed in percentage for all variables but the temperature, which is expressed in °C. The maximum deviations obtained for the cooling capacity and the consumption of the compressor are +2.24% and −0.83%, respectively. Furthermore, in Fig. 7 the COP of the refrigeration test bench is represented as a function of the discharge pressure for both experimental an simulated data. It clearly shows that the model is able to predict the optimum value for the discharge pressure and follows the tendency of the experimental tests. This ability to follow real tendencies in addition to the low deviations obtained between experimental and simulated data for the most important outputs, manifests that the base cycle model properly represents the behaviour of the experimental refrigeration test bench. Therefore, the base cycle model is validated and can be used in a more complex computational model where the behaviour of the TESC is introduced.

**Table 5**
Comparative between experimental and simulated data of the base cycle model $T_{evap} = -10$ °C $T_{amb} = 30$ °C and $RH_{amb} = 55\%$.

| Compared variable | | $P_{gc}$ (bar) 82.1 | 85.0 | 86.6 | 88.9 | 93.8 |
|---|---|---|---|---|---|---|
| $T_{evap\ out}$ (°C) | exper. | −6.31 | −6.34 | −6.30 | −6.37 | −6.33 |
| | simul. | −6.18 | −6.22 | −6.19 | −6.25 | −6.22 |
| Diff. $T_{evap\ out}$ (°C) | | +0.13 | +0.12 | +0.11 | +0.12 | +0.11 |
| $T_{comp\ in}$ (°C) | exper. | 5.61 | 5.48 | 5.79 | 5.51 | 5.64 |
| | simul. | 5.74 | 5.61 | 5.90 | 5.63 | 5.75 |
| Diff. $T_{comp\ in}$ (°C) | | +0.13 | +0.12 | +0.11 | +0.12 | +0.11 |
| $T_{comp\ out}$ (°C) | exper. | 80.66 | 82.22 | 82.80 | 84.66 | 86.46 |
| | simul. | 79.19 | 81.27 | 82.26 | 84.03 | 85.68 |
| Diff. $T_{comp\ out}$ (°C) | | −1.47 | −0.94 | −0.54 | −0.63 | −0.78 |
| $T_{gc\ out}$ (°C) | exper. | 33.30 | 32.60 | 32.20 | 31.95 | 31.75 |
| | simul. | 33.62 | 32.91 | 32.69 | 32.33 | 32.18 |
| Diff. $T_{gc\ out}$ (°C) | | +0.32 | +0.31 | +0.49 | +0.38 | +0.43 |
| $P_{evap}$ (bar) | exper. | 26.64 | 26.57 | 26.56 | 26.54 | 26.58 |
| | simul. | 26.57 | 26.50 | 26.49 | 26.46 | 26.50 |
| Diff. $P_{evap}$ (%) | | −0.27 | −0.30 | −0.27 | −0.29 | −0.30 |
| $\varepsilon_{gc}$ (0 − 1) | exper. | 0.920 | 0.938 | 0.949 | 0.956 | 0.962 |
| | simul. | 0.910 | 0.930 | 0.937 | 0.947 | 0.952 |
| Diff. $\varepsilon_{gc}$ (%) | | −1.06 | −0.88 | −1.27 | −0.98 | −1.05 |
| $\dot{m}_{CO2}$ (kg/h) | exper. | 7.327 | 7.108 | 7.049 | 6.794 | 6.366 |
| | simul. | 7.278 | 7.070 | 6.979 | 6.794 | 6.620 |
| Diff. $\dot{m}_{CO2}$ (%) | | −0.67 | −0.54 | −1.00 | +0.01 | +3.99 |
| $\dot{Q}_0$ (W) | exper. | 276.68 | 284.04 | 289.01 | 288.65 | 284.52 |
| | simul. | 274.33 | 288.28 | 290.63 | 292.11 | 290.89 |
| Diff. $\dot{Q}_0$ (%) | | −0.85 | +1.49 | +0.56 | +1.20 | +2.24 |
| $\dot{W}_{Comp}$ (W) | exper. | 272.10 | 275.33 | 279.50 | 281.51 | 287.33 |
| | simul. | 272.86 | 276.78 | 278.48 | 281.82 | 284.93 |
| Diff. $\dot{W}_{Comp}$ (%) | | +0.28 | +0.53 | −0.37 | +0.11 | −0.83 |
| $COP$ | exper. | 1.017 | 1.032 | 1.034 | 1.025 | 0.990 |
| | simul. | 1.005 | 1.042 | 1.044 | 1.037 | 1.021 |
| Diff. $COP$ (%) | | −1.13 | +0.96 | +0.93 | +1.09 | +3.09 |

### 3.2. Thermoelectric refrigeration model

The computational model represents a thermoelectric refrigeration system using an electrical analogy, it is based on a previously published and validated model in which the most important outputs are predicted with deviations lower than ±10% [27]. The model, that has been adapted for this application, uses the implicit finite difference method as it has been proven reliable for thermoelectric systems in applications such as cooling [28], waste heat recovery [29], or generation using geothermal energy [30]. The implicit finite difference method does not

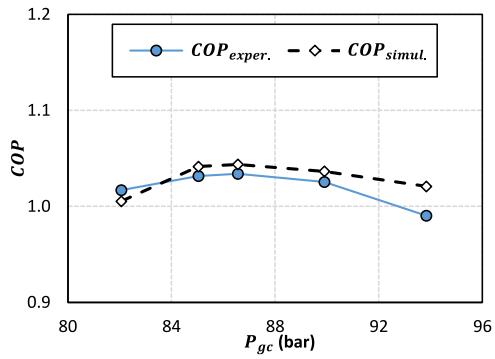


**Fig. 7.** COP of the refrigeration base cycle as a function of the discharge pressure for experimental and simulated data.

require any restriction either on the time step or the mesh size to converge and heat transfer is based in a set of partial differential equations based on the conservation laws and Fourier's law of heat conduction. The system needs to be discretized in a certain number of nodes and the equations are introduced for each node and the connected additional nodes. To comply with the finite difference method, the system is assumed one dimensional and is discretized homogeneously in thermal resistances. It is coded in Matlab, takes into account the effect of the $CO_2$ cooling in each block, the influence of the heat exchangers, the 4 thermoelectric effects (Peltier, Thomson, Seebeck and Joule effect) and considers temperature dependent thermoelectric properties.

The thermoelectric refrigeration model simulates the cooling produced on a $CO_2$ mass flow when flowing through a thermoelectric subcooler system as the one described in Section 2.2. The model calculates temperature distribution at the TESC, power consumption of the thermoelectric subcooler ($\dot{W}_{TESC}$) and heat flux extracted from the refrigerant ($\dot{Q}_{TESC}$), among others. In order to obtain higher precision, the model calculates the subcooling produced on each of the 4 subcooling blocks separately.

The inputs needed to solve each subcooling block are the following: average temperature of the $CO_2$ at the subcooling block ($T_{CO2}$), pressure of the $CO_2$ at the subcooling block ($P_{CO2}$), mass flow of the $CO_2$ ($\dot{m}_{CO2}$), ambient temperature ($T_{amb}$), voltage supplied to the TEMs ($V_{TEM}$) and voltage supplied to the fans of the finned heat exchangers ($V_{fan}$).

Each block of the TESC is discretized in 16 nodes, Fig. 8 shows the schematic of the electric analogy. It includes the finned heat exchangers with the ambient, the thermoelectric modules and the copper block heat exchangers with the refrigerant. The ambient is represented by node 1, the $CO_2$ by node 16 and the thermoelectric module is defined from nodes 3 to 14. The finned heat exchangers and the copper block are defined by $R_{amb\ hx}$ and $R_{CO2\ hx}$, respectively. $R_{amb\ cont}$ and $R_{CO2\ cont}$ represent the thermal contact resistance between the TEMs and the heat exchangers, and lastly, $R_{ins}$ defines the thermal bridge between both heat exchangers through the insulation material.

Eq. (13) shows the second order polynomial function used to introduce the resistance of the finned heat exchangers in the model. The heat exchangers have been thermally characterized under laboratory conditions ($T_{amb} = 30\,°C$ and $RH_{amb} = 55\%$), obtaining the thermal resistance ($R_{amb\ hx}$) as a function of the voltage supplied to the fans with maximum deviation of 8.5%.

$$R_{amb\ hx} = 1.3518 - 0.1648 \cdot V_{fan} + 0.0069 \cdot V_{fan}{}^2 \tag{13}$$

The thermal contact resistances between the TEMs and the heat exchangers is introduced using Eq. (14), where the thermal impedance ($Z_{tim} = 5.6 \cdot 10^{-5}\ m^2K/W$) is obtained through experimental data from previous studies [31,32], resulting in a thermal resistance of 0.035 K/W.

$$R_{amb\ cont} = R_{amb\ CO2} = \frac{Z_{tim}}{A_{tim}} \tag{14}$$

From node 3 to 14 the TEM is represented, nodes 3 and 14 define the hot and cold ceramic plate of the TEMs while nodes 4 to 13 represent the junctions and the thermoelectric materials. The 4 thermoelectric effects (Seebeck, Peltier, Thomson and Joule) are taken into account as shown in Eqs. (15)–(18). The 3 dimensional Fourier law of heat conduction shown in Eq. (19) is also introduced in the finite difference method to calculate the heat fluxes that appear on the studied system [27].

$$\alpha_{AB} = \frac{dE}{dT} = \alpha_A - \alpha_B \tag{15}$$

$$\dot{Q}_{Peltier} = \pm\, \pi_{AB} I = \pm\, IT(\alpha_A - \alpha_B) \tag{16}$$

$$\dot{Q}_{Thoms.} = -\sigma \vec{I}(\overrightarrow{\Delta T}) \tag{17}$$

$$\dot{Q}_{Joule} = R_0 I^2 \tag{18}$$

$$\rho c_p \frac{\partial T}{\partial t} = k\left(\frac{\partial^2 T}{\partial x^2} + \frac{\partial^2 T}{\partial y^2} + \frac{\partial^2 T}{\partial z^2}\right) + \bar{q} \tag{19}$$

The thermal resistance of the copper block heat exchanger ($R_{CO2\ hx}$) is calculated using the heat transfer coefficient and the area as in equation Eq. (20). The heat transfer coefficient is calculated using Gnielinski correlation for internal forced convection, presented in Eq. (21) [33] and the internal heat exchange area corresponds to $0.0037\,m^2$.

$$R_{CO2\ hx} = \frac{1}{A_{CO2\ hx} \cdot hc_{CO2\ hx}} \tag{20}$$

$$Nu = \frac{(f/8)(Re - 1000)Pr}{1 + 12.7(f/8)^{0.5}(Pr^{2/3} - 1)} \tag{21}$$

Finally, the thermal resistance of the insulation ($R_{ins}$) is defined as in Eq. (22) [34].

$$R_{ins} = \frac{e_{ins}}{k_{ins} \cdot A_{ins}} \tag{22}$$

By an iterative process using the implicit finite difference method and taking into account all the presented equations, the model is able to calculate temperature distribution, heat fluxes, consumption of the thermoelectric modules and consumption of the fans for the subcooling block.

### 3.3. Basic operation and interaction between models

The complete model simulates a transcritical carbon dioxide cycle that works with a thermoelectric subcooling system. In this section, the working principles and the interactions between both submodels (base cycle model and thermoelectric refrigeration model) are described. Fig. 9 shows an schematic of the basic operation of the computational tool.

The simulation process of the whole system starts by solving the vapour compression system. For that, the base cycle is resolved until the temperature at the outlet of the gas cooler is obtained, at that point, the thermoelectric refrigeration model calculates the cooling produced at the stream of $CO_2$. Lastly, energetic calculus are performed using the outputs obtained from both submodels.

The necessary inputs to start the calculus are the ones the base cycle model requires: evaporation level ($T_{evap}$), useful superheating ($USH$), non-useful superheating ($NUSH$), gas-cooler pressure ($P_{gc}$) and ambient temperature ($T_{amb}$). The relevant outputs obtained from the base cycle model are: power consumption at the compressor ($\dot{W}_{comp}$), mass flow of $CO_2$ through the installation ($\dot{m}_{CO2}$), temperature at the outlet of the gas-cooler ($T_3$) and enthalpy at the outlet of the evaporator ($h_8$) which are obtained as described in Section 3.1.

At this point the temperature at the outlet of the gas-cooler equals the inlet temperature of the subcooling system, and, as the subcooling system is discretized in 4 blocks, this temperature equals the inlet of the first block of the subcooling system ($T_{block\ 1\ in}$).

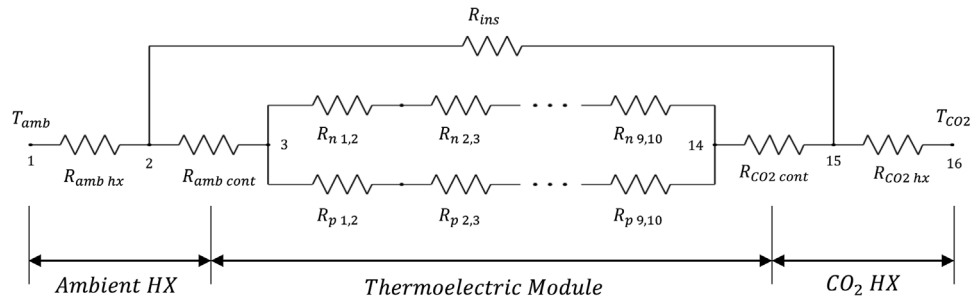


**Fig. 8.** Thermal–electric analogy of the thermoelectric subcooler block.

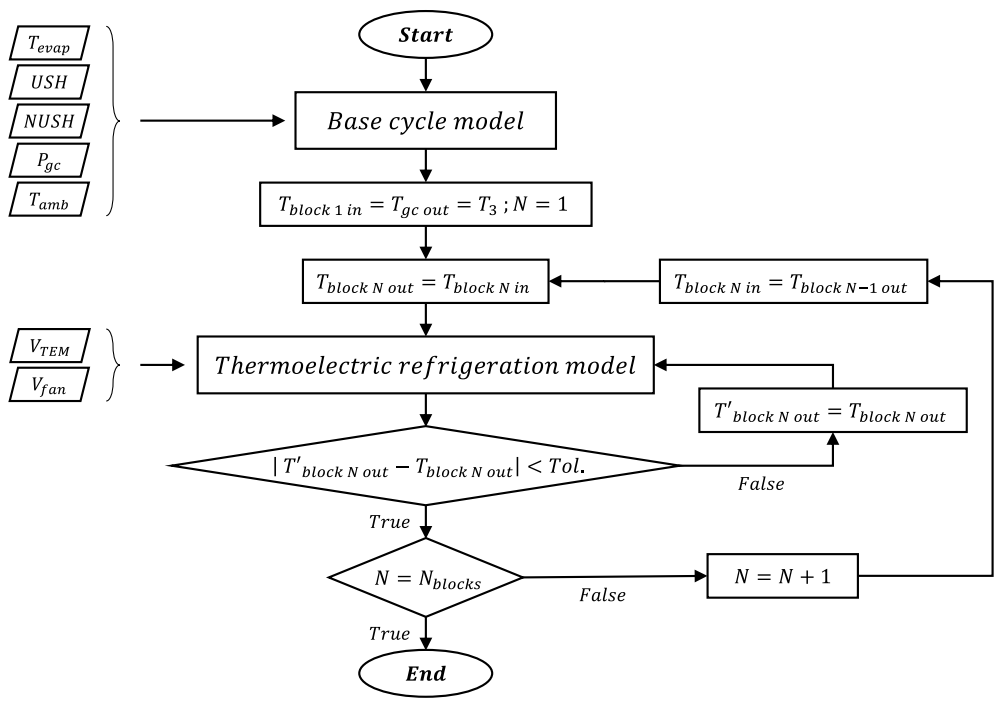


**Fig. 9.** Basic operation schematic of the computational model.

To solve each subcooling block, average temperature of the $CO_2$ ($T_{CO2}$) at the block is needed to start the iterative process. This temperature is obtained assuming the outlet of the subcooling block, to start the iterative process and only for the first step, temperature at the outlet of the subcooling block ($T_{block\ N\ out}$) equals temperature at the inlet of the block ($T_{block\ N\ in}$). Average temperature for the $CO_2$ is calculated and introduced in the thermoelectric refrigeration model along with the rest of the required inputs: pressure of the $CO_2$ at the subcooling block (same as the discharge pressure), ambient temperature (already introduced), mass flow of the $CO_2$ (calculated using the base cycle model), voltage supplied to the TEMs ($V_{TEM}$) and voltage supplied to the fans of the finned heat exchangers ($V_{fan}$). The outputs obtained from the thermoelectric refrigeration model for the subcooling block are: heat extracted from the $CO_2$ ($\dot{Q}_{block\ N}$), power consumption of the TEMs ($\dot{W}_{TEM\ N}$) and temperature distribution.

The calculated temperature at the outlet of the subcooling block ($T'_{block\ N\ out}$) is obtained using the heat extracted from the $CO_2$ as shown in Eq. (24) where the specific heat is calculated for the average temperature at the subcooling block.

$$T'_{block\ N\ out} = T_{block\ N\ in} - \frac{\dot{Q}_{block\ N}}{\dot{m}_{CO2} \cdot c_{p\ CO2}} \tag{23}$$

This calculated temperature at the outlet of the subcooling block is compared with the previously assumed temperature. If the difference between both temperatures is higher than a tolerance, which is set to 0.001 K, the block is calculated again assuming the temperature at the outlet of the subcooling block equals the calculated temperature from the last iteration. This process is repeated until the model converges and the subcooling block is completely solved obtaining temperature distribution, heat extracted, power consumption of the TEMs and power consumption of the fans.

Then, temperature at the inlet of the next block equals temperature at the outlet of the current block and the calculation process is repeated until all subcooling blocks are solved. At this point, energetic calculus are performed for the whole refrigeration system. Power consumption of the whole thermoelectric system is obtained adding the power consumption from the fans and the TEMs for all the subcooling blocks. Enthalpy at the outlet of the subcooling system ($h_4$) is calculated using Refprop v9.1. The enthalpy of points 5, 6 and 7 is the same as point 4 and therefore the cycle is resolved. Finally, cooling power and COP of the whole system are obtained using Eqs. (11) and (12).

## 4. Validation

In order to assess the reliability of the computational model, simulated data is compared with experimental data obtained from the tests explained in Section 2.4. First, the relative error between experimental and simulated data is compared for the principal outputs: cooling power, power consumption of the compressor, power consumption of

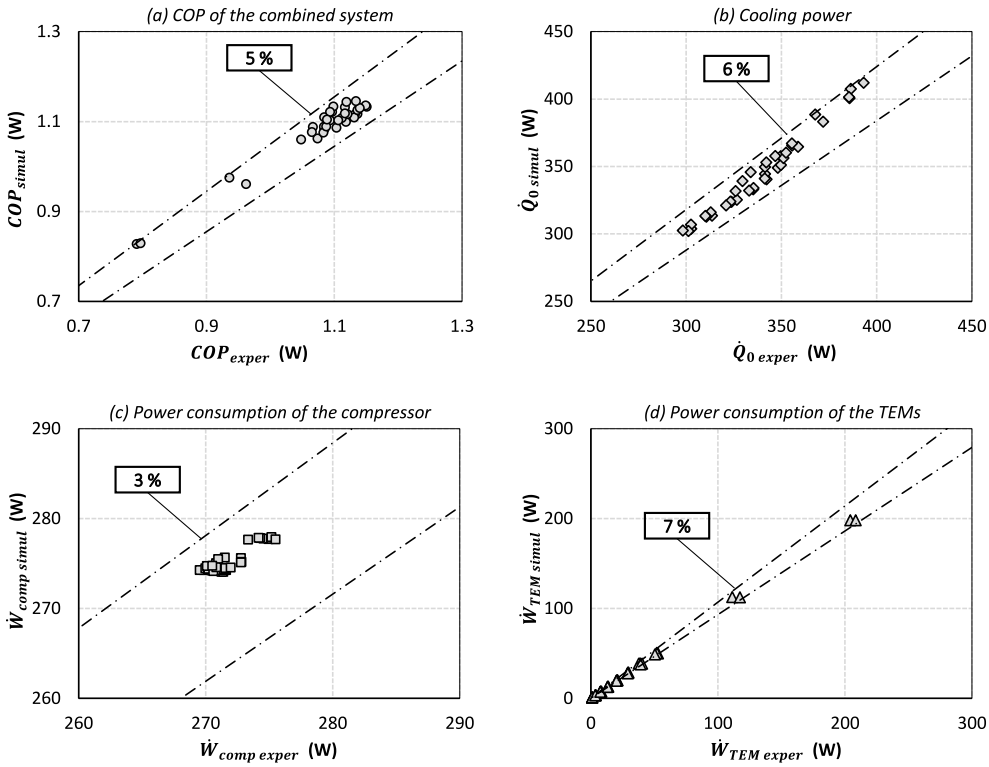


**Fig. 10.** Relative error between the computational model and experimental data for: COP of the combined system (a), cooling power (b), power consumption of the compressor (c) and power consumption of the TEMs (d).

the thermoelectric modules and COP of the combined system. Then, deviations for the rest of the outputs studied are presented in Table 6. Lastly, the ability of the computational model to predict real tendencies is tested.

Fig. 10 shows the relative error for the main outputs of the computational model. The COP of the transcritical $CO_2$ cycle with thermoelectric subcooler, being the most relevant output, presents deviations between the ±5%. Cooling power, power consumption of the compressor and power consumption of the TEMs present deviations between the ±6%, ±3% and ±7%, respectively. In addition, Table 6 collects many more variables that are compared to assess the reliability of the simulations. The values that the variables acquire during the experimental test are introduced in the column experimental range and the deviation is expressed as the maximum difference in percentage for all the variables but temperatures, which is expressed in differential units. It is important to highlight that the maximum deviations for most of the variables are obtained under not optimum working conditions such as when the TESC is supplied with very low or high voltages or for extreme gas-cooler pressures. This is clearly expressed for the subcooling in Table 6, where the subcooling is presented for 3 different intervals of voltage supplied to the TEMs. These low deviations alongside the small dispersion of the data shows high reliability for the computational model.

The COP of the whole system and the COP of the TESC, which is defined by Eq. (24), is compared between experimental and simulated data to test the reliability of the model to follow real tendencies. The comparative is represented in Fig. 11 for 2 different pressures of the gas cooler (83 and 86 bar) and a fixed voltage for the fans of the TESC (12 V). Experimental data clearly shows that the COP of both the whole system and the TESC first increases and then decreases, reaching an optimum value around 1.5 to 2 V for the voltage of the TEMs. When the voltage supplied to the TEMs is low, the COP of the TEM is very high but the consumption of the fans penalizes the COP drastically, resulting in a low COP. As the voltage supplied to the TEMs increases the subcooling produced increases, the COP of the TEMs decreases and

**Table 6**
Deviations of the studied variables of the computational model.

| Variable (unit) | Experimental range | Maximum deviation |
|---|---|---|
| $T_{comp\ out}$ (°C) | 79.76–83.63 | 1.13 °C |
| $T_{gc\ out}$ (°C) | 32.32–33.28 | 0.22 °C |
| $T_{TESC\ out}$ (°C) | 13.88–31.40 | 1.17 °C |
| $T_{TEM\ hot}$ (°C) | 32.44–48.86 | 4.27 °C |
| $T_{TEM\ cold}$ (°C) | 11.36–32.54 | 1.98 °C |
| $Sub_{TESC\ 0.5-1V}$ (°C) | 1.40–3.27 | 0.44 °C |
| $Sub_{TESC\ 1.5-2.5V}$ (°C) | 3.90–7.92 | 0.58 °C |
| $Sub_{TESC\ 3-8V}$ (°C) | 7.32–19.24 | 1.24 °C |
| $\varepsilon_{gc}$ (0–1) | 0.920–0.943 | 0.82% |
| $\dot{m}_{CO2}$ (kg/h) | 6.642–7.226 | 5.46% |
| $\dot{Q}_{TESC}$ (W) | 14.85–133.30 | 8.77% |
| $\dot{Q}_0$ (W) | 298.26–417.18 | 5.62% |
| $\dot{W}_{TEM}$ (W) | 0.9–208.5 | 6.73% |
| $\dot{W}_{comp}$ (W) | 269.53–276.56 | 1.75% |
| $COP$ | 0.79–1.15 | 4.63% |

the effect of the consumption of the fans becomes less relevant and therefore, and optimum value for the voltage supplied between these effects is obtained. The comparative exhibits great matching between experimental and simulated data as the tendency is properly followed by the computational model for different discharge pressures.

$$COP_{TESC} = \frac{\dot{Q}_{TESC}}{\dot{W}_{TESC}} = \frac{\dot{Q}_{TESC}}{\dot{W}_{TEM} + \dot{W}_{fan}} \tag{24}$$

Lastly, the effect of the voltage supplied to the fans of the finned heat exchangers is tested for the computational model. Experimentally, an increase on the voltage supplied to the fans results in a lower thermal resistance of the finned heat exchanger with the air. This, decreases the temperature gradient on the TEM and hence, increases the COP of the TEMs and, as a result, the subcooling produced by the thermoelectric system rises. Fig. 12 represents the subcooling produced by the thermoelectric system as a function of the voltage supplied to the fans for various voltages supplied to the TEMs. The model clearly

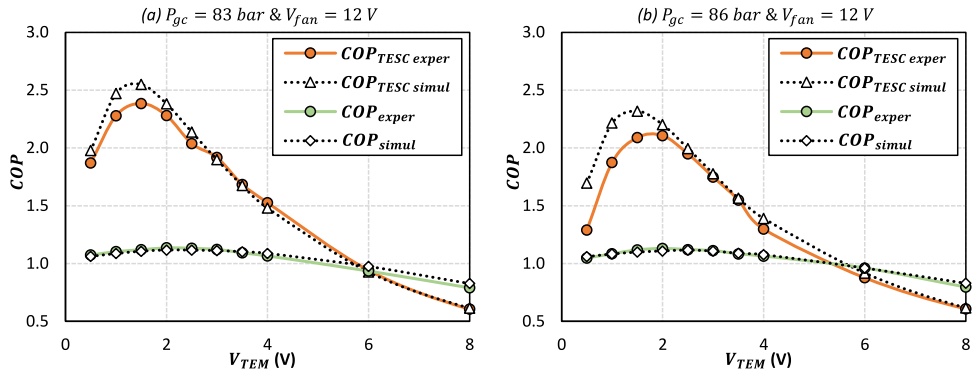


**Fig. 11.** Comparative between experimental and simulated, COP of the whole system and COP of the TESC as a function of the voltage supplied to the TEMs for: (a) $P_{gc}$ = 83 bar; $V_{fan}$ = 12 V and (b) $P_{gc}$ = 86 bar; $V_{fan}$ = 12 V.

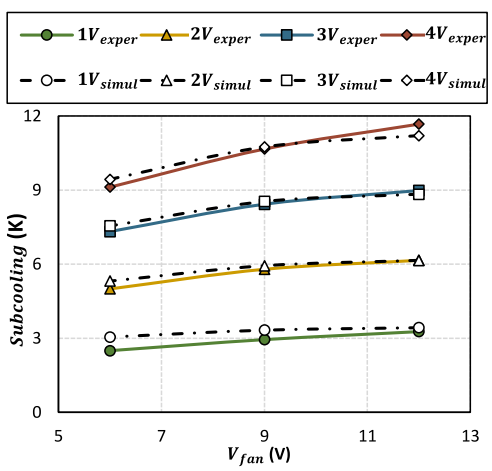


**Fig. 12.** Subcooling produced at the thermoelectric system as a function of the voltage supplied to the fans for experimental and simulated data ($P_{gc}$ = 83 bar).

follows the real tendency of increasing the subcooling as the voltage supplied to the fans increases for different voltages supplied to the TEMs.

The reliability of the computational model developed to simulate experimental behaviour has been tested. Deviations for the main outputs are low (between the ±7 %) and it has been proved that the computational tool is able to properly follow real tendencies. Therefore, the computational model developed is able to properly represent the behaviour of a carbon dioxide transcritical vapour compression cycle with a thermoelectric subcooling system. Consequently, the computational tool developed is able to aid in the design and optimization of vapour compression systems with thermoelectric subcoolers, been able to predict optimum working conditions of the combined system.

## 5. Optimization of the number of TEMs

The amount of TEMs to use in a thermoelectric subcooler is an important subject to address. On the one hand, when using few TEMs the subcooling degree produced is low with little effect on the whole system. On the other hand, when many TEMs are used, the subcooling degree increases alongside the extra consumption, decreasing the global efficiency drastically. Using the computational model and altering the number of TEMs used in the subcooling system, an study to optimize the number of TEMs for the current facility is performed.

The following inputs are introduced as a fixed value in the computational model: ambient temperature (30 °C), evaporation level (−10 °C), useful superheating (4 K), non useful superheating (12 K) and voltage supplied to the fans of the finned heat exchanger (12 V). The discharge pressure of the system is modified from 80 to 90 bar in 0.1 bar increments, the voltage supplied to the TEMs goes from 0.1 to 6 V in 0.1 V increments and lastly, the number of TEMs is modified from 2 to 24 in increments of 2. The combination of this variables generates 72720 simulations that are calculated with the complete computational model. Fig. 13 shows the optimum COP obtained for each number of TEMs, each value is obtained at a different discharge pressure and voltage supplied to the TEMs. The optimum cases are shown in detail in Table 7, it is clear to appreciate that as the number of TEMs increases the optimal COP is obtained for lower discharge pressures and lower voltage supplied to the TEMs. On the contrary, the optimal subcooling degree increases as the number of TEMs increases. The optimal simulated COP obtained is 1.1744, which represents an improvement of 2 % from the best experimental data acquired, this value is obtained for a discharge pressure of 82.5 bar a subcooling degree of 11.7 K and 2.1 V supplied to 16 TEMs.

Fig. 14 shows the optimal COP as a function of the voltage supplied to the TEMs and the number of TEMs. Each point is represented for the optimal pressure for that amount of TEMs and voltage supplied to them. The 3D graphic clearly shows that the voltage supplied to the TEMs needs to be set properly in order to obtain significant increases in the COP of the refrigeration cycle.

Experimental results of the inclusion of a thermoelectric subcooling system that uses 8 TEMs in a carbon dioxide transcritical vapour compression cycle produced a COP of 1.151 which traduces in an improvement of 11.3 % on the global COP of the combined system in comparison to the base cycle [13]. Using the computational model to optimize the number of TEMs, a COP of 1.1744 has been predicted when using 16 TEMs, which represents an improvement of 13.6 % in comparison to the experimental base cycle. These results clearly show that the improvement produced when using a thermoelectric subcooling system can be optimized and even greater improvements in the COP of the combined system can be obtained with proper design and operation.

## 6. Conclusions

In this work, a computational model able to predict the performance of a transcritical carbon dioxide vapour compression cycle with a thermoelectric subcooling system has been developed. The model takes into account working principles of base vapour compression systems, effect of the heat exchangers of the subcooling system, thermal contact resistances, temperature dependent thermoelectric properties and the 4 thermoelectric effects. It has been validated using previously experimental data, showing deviations for the coefficient of performance, cooling power, power consumption of the compressor and power consumption of the thermoelectric modules between the ±5 %, ±6 %, ±3 % and ±7 %, respectively. The low deviations obtained alongside the

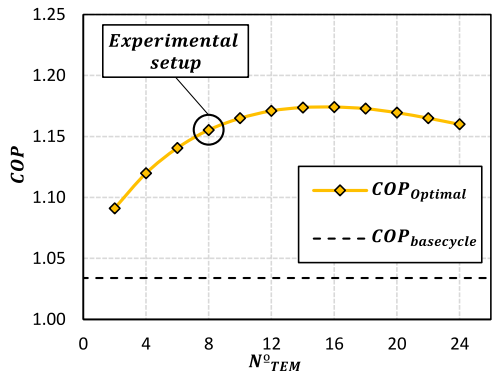


**Fig. 13.** Optimal simulated COP as a function of the number of TEMs. $T_{amb} = 30\,°C$, $RH_{amb} = 55\,\%$, $T_{evap} = -10\,°C$, $USH = 4$ K, $NUSH = 12$ K and $V_{fan} = 12$ V.

**Table 7**
Optimal simulated cases for each number of TEMs.

| TEMs (#) | COP | $P_{gc}$ (Bar) | $V_{TEMs}$ (V) | $\dot{Q}_0$ (W) | $\dot{Q}_{0\ TESC}$ (W) | $\dot{W}$ (W) | $\dot{W}_{comp}$ (W) | $\dot{W}_{TESC}$ (W) | $Sub.$ (K) | ΔCOP (%) |
|---|---|---|---|---|---|---|---|---|---|---|
| 2 | 1.0911 | 86.2 | 3.0 | 314.26 | 21.91 | 288.0 | 277.9 | 10.1 | 2.42 | 5.5 |
| 4 | 1.1198 | 85.6 | 2.8 | 330.84 | 39.58 | 295.4 | 277.2 | 18.2 | 4.57 | 8.3 |
| 6 | 1.1406 | 84.8 | 2.7 | 344.86 | 54.99 | 302.3 | 276.5 | 25.9 | 6.53 | 10.3 |
| 8 | 1.1554 | 84.4 | 2.5 | 354.35 | 66.25 | 306.7 | 275.7 | 31.0 | 7.92 | 11.7 |
| 10 | 1.1650 | 83.8 | 2.4 | 363.13 | 76.85 | 311.7 | 275.1 | 36.6 | 9.24 | 12.7 |
| 12 | 1.1711 | 83.4 | 2.3 | 369.96 | 85.89 | 315.9 | 274.4 | 41.5 | 10.28 | 13.3 |
| 14 | 1.1738 | 82.8 | 2.2 | 375.09 | 93.72 | 319.5 | 273.7 | 45.8 | 11.07 | 13.5 |
| 16 | 1.1742 | 82.6 | 2.1 | 379.06 | 99.60 | 322.8 | 273.3 | 49.5 | 11.70 | 13.6 |
| 18 | 1.1729 | 82.2 | 2.0 | 381.64 | 105.15 | 325.4 | 272.7 | 52.7 | 12.09 | 13.4 |
| 20 | 1.1696 | 81.8 | 1.9 | 383.42 | 108.63 | 327.8 | 272.4 | 55.4 | 12.37 | 13.1 |
| 22 | 1.1651 | 81.6 | 1.8 | 384.13 | 112.25 | 329.6 | 271.9 | 57.7 | 12.47 | 12.7 |
| 24 | 1.1600 | 81.4 | 1.8 | 387.78 | 119.31 | 334.3 | 271.5 | 62.8 | 13.06 | 12.2 |

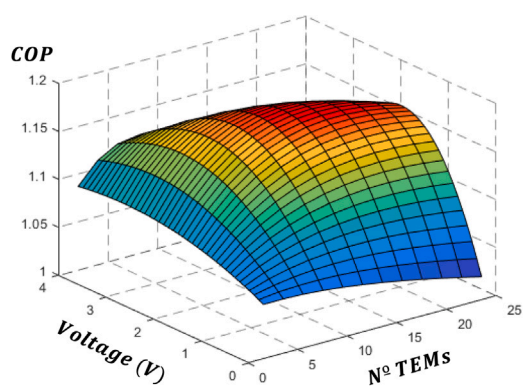


**Fig. 14.** Optimal simulated COP as a function of the number of TEMs and the voltage supplied to the TEMs.

ability of the computational tool to predict real tendencies have proved the reliability of the model.

An optimization of the experimental setup has been performed focusing on the number of thermoelectric modules. From the simulations performed the optimal configuration is obtained for 16 thermoelectric modules supplied with 2.1 V and a discharge pressure of 82.5 bar, resulting in a coefficient of performance of 1.1744, which represents an improvement of 13.6 % in comparison to the experimental base cycle. Simulations show that when increasing the number of thermoelectric modules, the optimal discharge pressure and the optimal supply voltage decreases.

The developed computational tool is able to predict the optimum configuration and operating conditions of the whole refrigeration plant. It is also capable of calculating the effect of a large amount of variables on the combined system such as: evaporation level, ambient temperature, cubic capacity of the compressor, efficiency of the gas cooler, number of thermoelectric modules, etc. Therefore, it is able to serve as a useful tool in the optimization of the operation settings and the design of thermoelectric subcooling systems for carbon dioxide refrigeration cycles.

## Declaration of competing interest

The authors declare that they have no known competing financial interests or personal relationships that could have appeared to influence the work reported in this paper.

## Acknowledgements

The authors would like to acknowledge the support of the Spanish Ministry of Science, Innovation and Universities, and European Regional Development Fund, for the funding under the RTI2018-093501-B-C21 and RTI2018-093501-B-C22 research projects. We would also like to acknowledge the support from the Education Department of the Government of Navarra, Spain with the *Predoctoral Grants for Phd programs of Interest to Navarra* and the Official School of Industrial Engineers of Navarre with the scholarship, Spain *Fuentes Dutor*.

## References

[1] G. Lorentzen, The use of natural refrigerants : a complete solution to the CFC/HCFC predicament (utilisation des frigorigénes naturels : une solution complete au probl me des CFC et des HCFC), Int. J. Refrig. Vol. 18 (3) (1995) 190–197.

[2] G. Lorentzen, J. Pettersen, A new, efficient and environmentally benign system for car air-conditioning, Int. J. Refriger. 16 (1) (1993) 4–12, http://dx.doi.org/10.1016/0140-7007(93)90014-Y.

[3] M.H. Kim, J. Pettersen, C.W. Bullard, Fundamental process and system design issues in CO2 vapor compression systems, Prog. Energy Combust. Sci. 30 (2) (2004) 119–174, http://dx.doi.org/10.1016/j.pecs.2003.09.002.

[4] A. Fartaj, D.S. Ting, W.W. Yang, Second law analysis of the transcritical CO2 refrigeration cycle, Energy Conver. Manag. 45 (13–14) (2004) 2269–2281, http://dx.doi.org/10.1016/J.ENCONMAN.2003.07.001.

[5] D. Sánchez, J. Patiño, R. Llopis, R. Cabello, E. Torrella, F.V. Fuentes, New positions for an internal heat exchanger in a CO2 supercritical refrigeration plant. Experimental analysis and energetic evaluation, Appl. Therm. Eng. 63 (1) (2014) 129–139, http://dx.doi.org/10.1016/j.applthermaleng.2013.10.061.

[6] J. Sarkar, N. Agrawal, Performance optimization of transcritical CO2 cycle with parallel compression economization, Int. J. Thermal Sci. 49 (5) (2010) 838–843, http://dx.doi.org/10.1016/j.ijthermalsci.2009.12.001.

[7] J. Catalán-Gil, L. Nebot-Andrés, D. Sánchez, R. Llopis, R. Cabello, D. Calleja-Anta, Improvements in CO2 booster architectures with different economizer arrangements, Energies 13 (5) (2020) http://dx.doi.org/10.3390/en13051271.

[8] Y.T. Ge, S.A. Tassou, Thermodynamic analysis of transcritical CO2 booster refrigeration systems in supermarket, Energy Convers. Manag. 52 (4) (2011) 1868–1875, http://dx.doi.org/10.1016/J.ENCONMAN.2010.11.015.

[9] D. Li, E.A. Groll, Transcritical CO2 refrigeration cycle with ejector-expansion device, Int. J. Refriger. 28 (5) (2005) 766–773, http://dx.doi.org/10.1016/j.ijrefrig.2004.10.008.

[10] T. Bai, J. Yu, G. Yan, Advanced exergy analyses of an ejector expansion transcritical CO2 refrigeration system, Energy Convers. Manag. 126 (2016) 850–861, http://dx.doi.org/10.1016/J.ENCONMAN.2016.08.057.

[11] Y. Zhu, C. Li, F. Zhang, P.X. Jiang, Comprehensive experimental study on a transcritical CO2 ejector-expansion refrigeration system, Energy Convers. Manag. 151 (2017) 98–106, http://dx.doi.org/10.1016/J.ENCONMAN.2017.08.061.

[12] B. Zhang, D. Zhao, Y. Zhao, H. Ji, L. Chen, L. Liu, Comparative analysis of typical improvement methods in transcritical carbon dioxide refrigeration cycle, in: Procedia Engineering, Vol. 205, Elsevier Ltd, Zhang2017, 2017, pp. 1207–1214, http://dx.doi.org/10.1016/j.proeng.2017.10.355.

[13] P. Aranguren, D. Sánchez, A. Casi, R. Cabello, D. Astrain, Experimental assessment of a thermoelectric subcooler included in a transcritical CO2 refrigeration plant, Appl. Therm. Eng. 190 (2021) 116826, http://dx.doi.org/10.1016/j.applthermaleng.2021.116826.

[14] L. Nebot-Andrés, J. Catalán-Gil, D. Sánchez, D. Calleja-Anta, R. Cabello, R. Llopis, Experimental determination of the optimum working conditions of a transcritical CO2 refrigeration plant with integrated mechanical subcooling, Int. J. Refriger. 113 (2020) 266–275, http://dx.doi.org/10.1016/j.ijrefrig.2020.02.012.

[15] B. Dai, H. Qi, S. Liu, M. Ma, Z. Zhong, H. Li, M. Song, Z. Sun, Evaluation of transcritical CO2 heat pump system integrated with mechanical subcooling by utilizing energy, exergy and economic methodologies for residential heating, Energy Convers. Manag. 192 (February) (2019) 202–220, http://dx.doi.org/10.1016/j.enconman.2019.03.094.

[16] B. Dai, S. Liu, K. Zhu, Z. Sun, Y. Ma, Thermodynamic performance evaluation of transcritical carbon dioxide refrigeration cycle integrated with thermoelectric subcooler and expander, Energy 122 (2017) 787–800, http://dx.doi.org/10.1016/j.energy.2017.01.029.

[17] X. Liu, R. Fu, Z. Wang, L. Lin, Z. Sun, X. Li, Thermodynamic analysis of transcritical CO2 refrigeration cycle integrated with thermoelectric subcooler and ejector, Energy Convers. Manag. 188 (February) (2019) 354–365, http://dx.doi.org/10.1016/j.enconman.2019.02.088.

[18] J. Sarkar, Performance optimization of transcritical CO2 refrigeration cycle with thermoelectric subcooler, Int. J. Energy Res. 37 (2) (2013) 121–128, http://dx.doi.org/10.1002/er.1879.

[19] K. Yazawa, S. Dharkar, O. Kurtulus, E.A. Groll, Optimum design for thermoelectric in a sub-cooled trans-critical CO2 heat pump for data center cooling, in: Annual IEEE Semiconductor Thermal Measurement and Management Symposium, 2015-April, 2015, pp. 19–24, http://dx.doi.org/10.1109/SEMI-THERM.2015.7100133.

[20] S. Jamali, M. Yari, F. Mohammadkhani, Performance improvement of a transcritical CO2 refrigeration cycle using two-stage thermoelectric modules in sub-cooler and gas cooler, Int. J. Refriger. 74 (2017) 105–115, http://dx.doi.org/10.1016/j.ijrefrig.2016.10.007.

[21] T.H. Kwan, Y. Shen, G. Pei, Multi-objective approach for the performance and economic optimization of the two TED sub-cooled trans-critical carbon dioxide cycle, Int. J. Refriger. 127 (2021) 89–100, http://dx.doi.org/10.1016/j.ijrefrig.2021.02.021.

[22] D. Astrain, P. Aranguren, A. Martínez, A. Rodríguez, M.G. Pérez, A comparative study of different heat exchange systems in a thermoelectric refrigerator and their influence on the efficiency, Appl. Therm. Eng. (2016) http://dx.doi.org/10.1016/j.applthermaleng.2016.04.132.

[23] G. Fraisse, J. Ramousse, D. Sgorlon, C. Goupil, Comparison of different modeling approaches for thermoelectric elements, Energy Convers. Manag. 65 (2013) 351–356, http://dx.doi.org/10.1016/J.ENCONMAN.2012.08.022.

[24] P. Aranguren, M. Araiz, D. Astrain, Auxiliary consumption: A necessary energy that affects thermoelectric generation, Appl. Therm. Eng. 141 (September 2017) (2018) 990–999, http://dx.doi.org/10.1016/j.applthermaleng.2018.06.042.

[25] D. Sánchez, P. Aranguren, A. Casi, R. Llopis, R. Cabello, D. Astrain, Experimental enhancement of a CO2 transcritical refrigerating plant including thermoelectric subcooling, Int. J. Refriger. 120 (2020) 178–187, http://dx.doi.org/10.1016/j.ijrefrig.2020.08.031.

[26] D. Sánchez, J. Catalán-Gil, R. Cabello, D. Calleja-Anta, R. Llopis, L. Nebot-Andrés, Experimental analysis and optimization of an R744 transcritical cycle working with a mechanical subcooling system, Energies 13 (12) (2020) http://dx.doi.org/10.3390/en13123204.

[27] A. Martinez, D. Astrain, A. Rodriguez, P. Aranguren, Advanced computational model for peltier effect based refrigerators, Appl. Therm. Eng. 95 (2016) 339–347, http://dx.doi.org/10.1016/j.applthermaleng.2015.11.021.

[28] A. Martínez, D. Astrain, A. Rodríguez, Dynamic model for simulation of thermoelectric self cooling applications, Energy 55 (2013) 1114–1126, http://dx.doi.org/10.1016/j.energy.2013.03.093.

[29] P. Aranguren, M. Araiz, D. Astrain, A. Martínez, Thermoelectric generators for waste heat harvesting: A computational and experimental approach, Energy Convers. Manag. 148 (2017) 680–691, http://dx.doi.org/10.1016/j.enconman.2017.06.040.

[30] L. Catalan, M. Araiz, P. Aranguren, D. Astrain, Computational study of geothermal thermoelectric generators with phase change heat exchangers, Energy Convers. Manag. 221 (April) (2020) 113120, http://dx.doi.org/10.1016/j.enconman.2020.113120.

[31] M. Araiz, L. Catalan, O. Herrero, G. Perez, A. Rofriguez, P. Aranguren, The importance of the assembly in thermoelectric generators, in: P. Aranguren (Ed.), Bringing Thermoelectricity Into Reality, 2018, http://dx.doi.org/10.5772/intechopen.71354.

[32] A. Rodriguez, G. Perez-Artieda, I. Beisti, D. Astrain, A. Martinez, Influence of temperature and aging on the thermal contact resistance in thermoelectric devices, 2020, http://dx.doi.org/10.1007/s11664-020-08015-y.

[33] V. Gnileinski, New equations for heat and mass transfer in turbulent pipe and channel flow, Int. Chem. Eng. 16 (2) (1976) 359–368.

[34] A.J. Chapman, Heat Transfer, fourth ed., Macmillan, 1984.